〈論 文〉 4-2-11

다층신경회로망을 이용한 NiH_2 전지 모델링 및 동작상태분석

崔載東, 黃永聖, 李鶴周, 成世鎭

Modeling and Operation Analysis of NiH_2 Battery using Multi-layer Neural Network

Jae-Dong Choi, Yeong-Seong Hwang, Hak-Ju Lee and Se-Jin Seong

요 약

위성의 전지는 위성의 수명과 직접적인 영향을 갖고 있으며 이것의 정상동작여부에 따라 위성의 안정적인 임무수행여부가 결정된다. 상대적으로 일반화된 셀 모델링의 최근 개발은 NiH2셀의 동특성을 시뮬레이션 하기 위한 기본적인 원리에 기반을 둔 접근방식이다. 그러나 이러한 일반적인 방정식을 통해 비선형성과 전력상태를 포함하는 전지 특성을 예측하는 것은 사실상 불가능하다.

본 연구에서는 다층신경회로망을 이용하여 비선형 특성을 갖는 니켈-하이드로진 전지 특성을 모델링 하였으며, 모델링된 상수값은 위성의 식기간 동안의 전지 전력상태 분석을 위해 사용되었다. 모델링 결과의 정확성을 확인하기 위해 니켈-하이드로진 전지 시험결과 분석자료와 비교 검토 되었다. 전지 동작모드는 정상동작모드와 실패모드로 나누어 분석되었다. 정상동작모드는 위성의 식기간 동안 아크젯 동작 여부에 의해 각각 분석되었으며, 또한 태양전지와 배터리 셀 일부의 고장으로 인한 실패모드에서의 전지 전력상태가 분석되었다.

ABSTRACT

A satellite batteries have direct impact on the life time of the satellites, and stable operation is decided by whether they are in the steady state operation or not. The recent development of a relatively generalized cell modeling approach is based on the fundamental principle to simulate the dynamic behavior of a nickel-hydrogen cell. In fact, the prediction of the battery characteristics which include the nonlinear and the power state via general equation are impossible.

In this study, NiH2 battery characteristics using a multi-layer neural network are modelled, and their results are used in the analysis of the battery power state during eclipse condition of satellites. Also, the result is compared to battery test results to identify the reliability of modelling. The battery operation modes are classified into normal and failure modes, respectively. The normal mode is analyzed during the eclipse with the arcjet burn and the failure mode with solar array and battery cell failure is analyzed too.

Key Words: Satellite Battery Power, NiH2 battery characteristics, Eclipse Operation Mode

1. INTRODUCTION

Satellite power system consists of solar array, solar array drive units, power control units which include solar array regulator and battery charger/discharger, the batteries and various loads. The solar array is the main power source of the satellite and the power control unit controls the power from the solar array and distributes to the loads. And the battery store the power during the daylight and also the power is

provided to the load from the battery during the eclipse[1].

In the power subsystem of a satellite, the battery directly affects the life time of the satellite, so stable operation is demanded. But the nickel-hydrogen battery has some limitation. Expansion of the nickel electrode, electrolyte redistribution, and pressure vessel leaks may limit the life of the nickel-hydrogen battery[2]. If the failure of battery cell occurs, the analysis of battery power state will be important data to decide the stable operation. Thus the modeling of battery with nonlinear characteristics has to precede to predict the state of battery.

But computer-based simulations of the performance of rechargeable battery cells typically have been very limited in the past. There are a number of reasons for insufficient progress in this area. First, all battery cells are relatively complex electrochemical systems, in which performance is dictated by a large number of interacting physical and chemical elements. Second, while specific chemical and physical changes within cell components are associated with degradation, there has been no generalized simulation architecture that enables the chemical and physical structure to be translated into the cell performance. The recent development of a relatively generalized cell modeling approach is based on fundamental principles to simulate the dynamic behavior of a nickel-hydrogen cell[3~5]. In fact, the prediction of the battery characteristics which include the nonlinear and the power state via a general equation are virtually impossible.

In this paper, the battery modeling using MNN(Multi-layer Neural Network) which is compatible to the system modeling with nonlinear characteristics is implemented, and the modeled numerical data are used for the analysis of battery state during eclipse. In order to validate the identification of the modeling the simulation results using modeled data are compared to battery state analysis results. Battery operation modes are analyzed for the normal and failure modes at the eclipse. The normal mode is analyzed for the eclipse which has 12 minutes arcjet thruster burn at the second eclipse. Furthermore, the failure mode which has solar cell string failure, solar cell circuit failure and battery cell failure is analyzed separately .

2. BATTERY MODELING

The purpose of battery modeling using a ANN(Artificial Neural Network) is to produce an exact solution via training of analysis result for each operational mode under the change of battery charge/discharge parameter. ANN represents a new structure which comes from the neuron transfer system. This presents a mathematical model which constitutes several layers with few neurons. It is also represented as a kind of net describing the relationship of the output for external input.

The most widely used architecture of the multi-layered networks is shown in Fig. 1. Backpropagation networks often have one or more hidden layers of sigmoid neurons followed by an output layer of linear neurons.

Multiple layers of neurons with nonlinear transfer functions allow the network to learn nonlinear and linear relationships between input and output layers.

ANN used for battery modeling is multi-layered networks by backpropagation, and it trains a nonlinear function by the backpropagation learning rule which has several hidden layers between input and output layers. In general, a multi-layered networks is calculated by

$$x_j^k = f\left(\Sigma \omega_{ji}^k + x_j^{k-1} B_j^k\right) = f\left(N_j\right) \tag{1}$$

where ω_{ji}^k are the weights between ith neuron of $k-1$th layer and the jth neuron of the kth layer, B_j^k is the biases of the jth neuron of the kth layer. Then, f is an active function of neuron in Sigmoid function type.

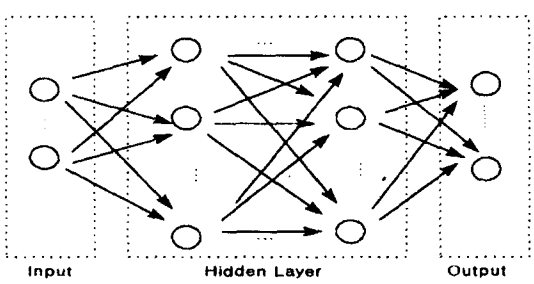

Fig. 1 Multi-layer Neural Network

The backpropagation learning rule can be used to adjust the weights and biases of networks in order to minimize the sum-squared error of the network. This is done by continually changing the values of the network weights and biases in the direction of steepest decent with respect to error.

For input pattern x_i, the changing value of the next step weight, Δw_{ji} is given by

$$\Delta\omega_{ji} = \eta\delta_j x_i \qquad (2)$$

where η is the learning rate, and

$\delta_j = (t_j - x_j) f`(N_j)$: j is output neuron

$= f`(N_j)\Sigma\delta_k w_{kj}$: j is hidden layer neuron

where t_j is the learning goal value and x_j is the output value of the j th neuron

2.1 Battery capacity modeling

Table 1 and 2 show the experimented data and characteristic data of the NiH_2 battery of Koreasat 3. The performance of battery is shown to be better at below 0℃. Fig 2 is the result of the neural network learning using the experimented data of Table 1 being estimated data at each different temperature point. The training was performed with 2 hidden layers and 5 neurons with a final root mean square error of about 0.001 between the target function and ANN outputs. A nonlinear characteristic of battery capacity is observed. By this experiment result and learning data, we can predict that Koreasat 3 battery has higher efficiency when the battery control mode is between 0℃ and -10℃.

Table 1 Capacity data of Koreasat 3 NiH_2 battery

		Max(AH)	Avg(AH)	Min(AH)
-10℃	AH/1.0V	129.1	128.0	126.9
	AH/1.1V	121.7	120.0	117.3
-5℃	AH/1.0V	126.2	124.7	122.5
	AH/1.1V	118.2	116.2	113.2
0℃	AH/1.0V	123.1	122.0	120.6
	AH/1.1V	110.0	116.0	114.8
10℃	AH/1.0V	116.1	114.7	112.8
	AH/1.1V	113.8	112.2	110.5
20℃	AH/1.0V	107.6	104.3	101.6
	AH/1.1V	105.8	102.6	100.0

2.2 Battery charge efficiency modeling

The instantaneous charge efficiency is determined by taking the derivative of the pressure with time. A linear pressure rise during charge represents 100 percent charge efficiency. As the pressure rise starts to drop off, the instantaneous charge efficiency drops off. Also, the charge efficiency is different according to the temperature[6].

For example, the charge efficiency improves at lower temperature. The overall charge efficiency is computed by integrating the area under the curve over the 16-hour charge period. The overall charge efficiency of Koreasat 3 is 87% . Also, the battery efficiency can be calculated by the voltage difference of battery under charge and discharge. It becomes about 87% when the ratio between charge and discharge voltage is 1.0. The 13% of remaining energy is dissipated by thermal effect. Figure 3 shows that the charge efficiency profile is different according to the temperature. Battery charge efficiency depends on the cell circumstance

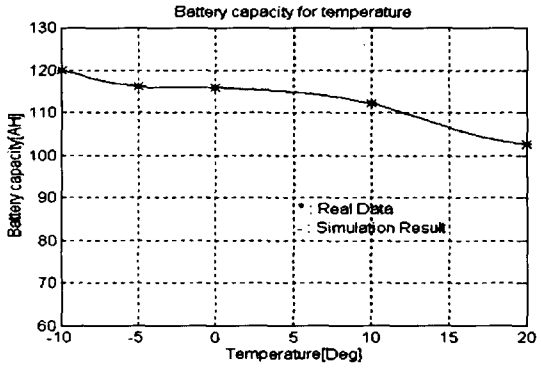

Fig. 2 Battery capacity modeling for temperature

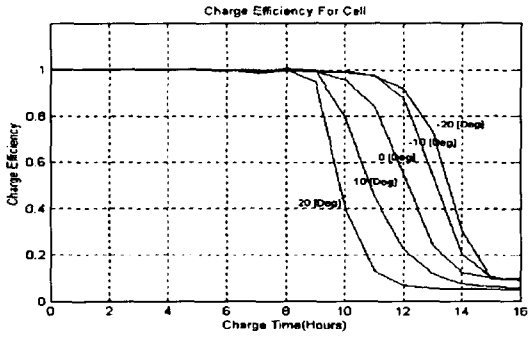

Fig. 3 Cell charge efficiency modeling for temperature(C/10)

temperature. As shown in Fig. 4, the temperature rising occurs after 7 hours at -10℃ or -20℃ since the charge started. The main reason of temperature rising is because the charge current changes by thermal effect caused by the charge efficiency drop. Thus, when the temperature of cell circumstance is over 0℃, the temperature rising rate is quicker at lower temperature. Fig. 5 shows the charge voltage profile at each different temperature. From the results of Figs. 3 and 4, the charge voltage at each different temperature is charged to 1.6V at -20℃ after passing 8 hours after charge started. On the contrary, the charge voltage at temperature over 20℃ reached only 1.46V because the charge efficiency is quickly dropped by the temperature rising. Thus the voltage at the end of charge is shown different as in Fig. 5. Similarly, when the battery discharge, the capacity of battery is higher at lower temperature. From the modeling results of battery charge efficiency which is shown from Figs. 3 to 5, we know that the battery charge efficiency is plotted differently according to the cell temperature, charge state and charge current state. The charge efficiency profiles for temperature and state of charge at C/10, C/20 are shown in Fig. 6 and 7. Firstly, Fig. 6(a) and (b) are data of battery cell efficiency with charge rate of C/10 and the training results using ANN, respectively. The charge efficiency for lower temperatures is almost 100% irrespective of the SOC(State of Charge). On the contrary, the charge efficiency at higher temperature is

Table 2 Characteristic data of Koreasat 3 NiH_2 battery

Parameter	Characteristic
· Battery Quantity	2 per spacecraft
· Cell per Battery	26 IPV
· Cell Type	100Ah Mantech (114Ahr actual)
· Max battery voltage (end of charge)	41.6V@ 100% SOC Ibc=10A
· Max battery voltage (beginning of discharge)	33.8V@ 100% SOC Ibc=10A
· Min battery voltage (end of discharge)	27.5V@ 20% SOC Ibc=100A
· Cell Pressure	950psi maximum
· Battery Temperature	-10 to +35 deg C
· C/D Ratio	1.3 On-Station

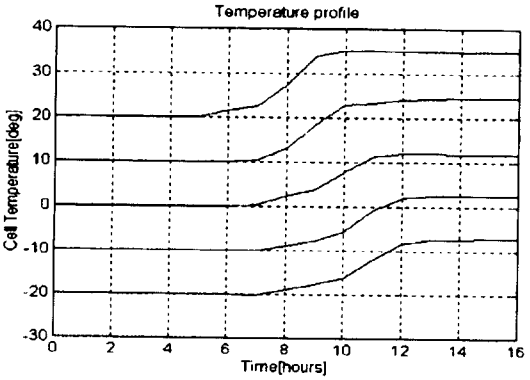

Fig. 4 Battery temperature profile for charge time (C/10)

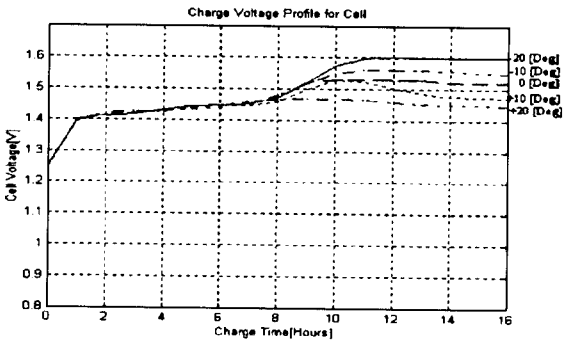

Fig. 5 Cell charge voltage modeling for charge time(C/2)

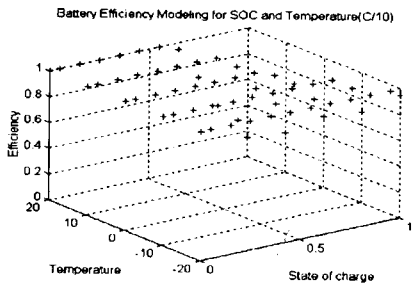

(a) Cell efficiency data

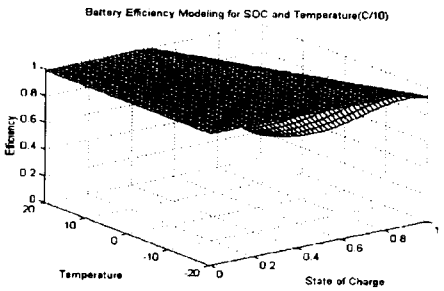

(b) Modeling result

Fig. 6 Battery efficiency modeling for temperature and state of charge(C/10)

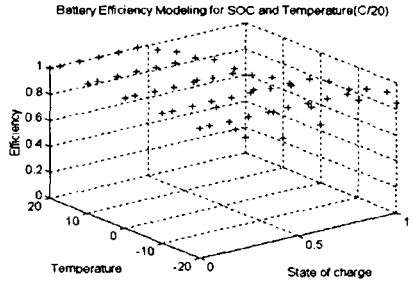

(a) Cell efficiency data

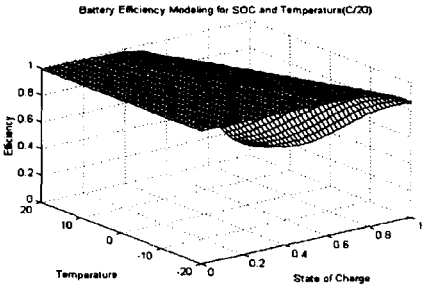

(b) Modeling result

Fig. 7 Battery efficiency modeling for temperature and state of charge(C/20)

dropped as soon as the charge state exceeds 50%.

3. BATTERY OPERATION MODE ANALYSIS

Battery power simulation according to the operational modes is conducted for the normal and failure modes during the eclipse with arcjet burn. The battery store power provided to the load during daylight which include arcjet burn for stationkeeping during eclipse. During the eclipse, the power is provided to the load only by the battery because power from a solar array is not available in the near autumnal equinox.

The battery and bus voltage of Koreasat 3 are set differently as shown in Fig. 8. Therefore, the battery voltage is stepped up to the bus voltage via battery discharger and distributed to the bus. On the contrary, the bus power is charged to the battery after the battery voltage step down during daylight[7].

3.1 Control Logic

In the battery operation simulation, battery capacity,

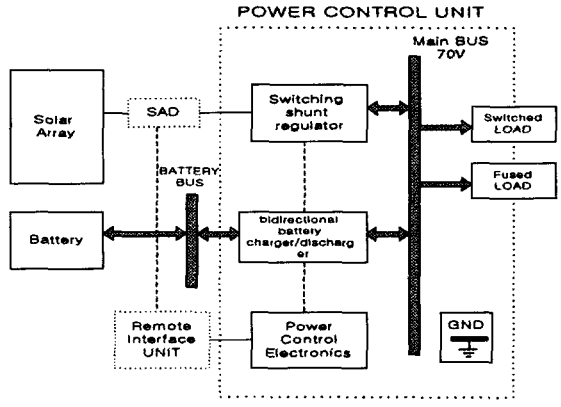

Fig. 8 Block diagram of the battery charge/discharge regulator

voltage, current and the state of charge are analyzed for the eclipse using battery neural data modelled in Section 2. And it is also analyzed for a worst case mode which can occur at the solar array string, circuit, and battery cell failure. Figure 9 is a control flow chart for the battery power analysis at the autumnal equinox. First, the current state of a satellite is set and then the initial input data are needed at each operation mode. The operation mode of the satellite by initial data is set and then temperature data at each mode is read so that the efficiency of the cell is calculated. After the calculation of cell efficiency and capacity, the state charge of cell is decided by that results. And it decides the cell voltage according to the charge state and the sum of cell voltage becomes the battery voltage. During the battery discharge, the change of battery capacity is as follows

$$AH_{CAP}(n+1) = AH_{CAP}(n) - \frac{P_{load}}{\left(V_{batbus}(n) - \frac{P_{load}}{P_{batbus}(n)} \times R_i \times Bat_{cap}\right)} \quad (4)$$

Similar to the charge, the battery capacity is decided by the battery discharge current which is changed by the load variation per minute unit. In Eq.(4) n represents the per minute unit, R_i is the interior impedance of the cell. The overall impedance of the battery cell of Koreasat 3, is 0.0364Ω. And P_{load} is the load power for arcjet burn or payload, V_{batbus} (n) is the

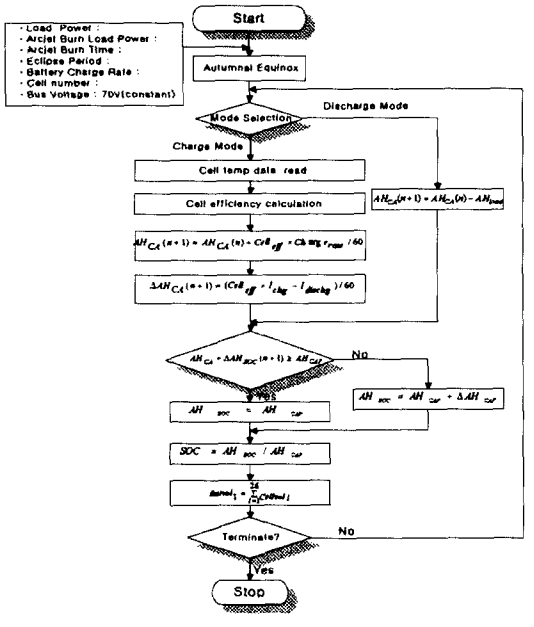

Fig. 9 Control flow chart for battery power analysis at autumnal equinox

sum of cell voltage and Bat_{cap} represents the battery capacity. After arcjet burn, the change of battery capacity during cell charging is given by

$$AH_{CAP}(n+1) = AH_{CAP}(n) + Cell_{eff} \times Charge\ \ rate/60 \quad (5)$$

Then the efficiency of the battery is decided by the modeling results of Figs. 6, 7 and the battery capacity changes from the data calculated by per minute unit.

From Eq. (4) and (5), the instantaneous value of SOC is calculated using the following expression

$$\Delta AH_{SOC} = \left(Cell_{eff} \times I_{chg} - I_{dschg}\right)/60 \quad (6)$$

From Eq. (6), it follows

$$AH_{SOC} + \Delta AH_{SOC} \geq AH_{cap},\ AH_{SOC} = AH_{cap} \quad (7)$$
$$AH_{SOC} + \Delta AH_{SOC} \langle AH_{cap},\ AH_{SOC} = AH_{cap} + \Delta AH_{SOC}$$

According to the above variation, SOC is calculated as follows

$$SOC = \frac{AH_{SOC}}{AH_{cap}} \quad (8)$$

where AH_{cap} is amp-hour battery capacity.

3.2 Eclipse normal mode analysis

This paper is analyzed for the autumnal equinox with the eclipse of maximum 72 minutes as the longest eclipse of Fig. 10. And the battery power state after arcjet burn is analyzed at the charge mode during 12 minutes. However, the arcjet burn time can change according to the charge state, but in this study, it is analyzed only for possible time of arcjet burn state during the battery charge uder maximum eclipse. Then, predicted operating temperature ranges of battery are shown in Table 3.

The power required by load is 4260 W during the eclipse, and under the arcjet burn event during the charge period it increases to 8700 W. Then the arcjet burn time can vary according to the battery operation state and eclipse period. Eclipse normal mode is implemented during 4320 minutes of 3 period. Each period includes the eclipse of maximum 72 minutes at the autumnal equinox and the charge rate of battery is set as C/18 after the eclipse. In Fig. 11(a), after the eclipse, the necessary charge state of battery reaches 100% before the next eclipse.

And the arcjet burn is implemented at the second period among three eclipse periods. Because the maximum arcjet time of the second period can be decided by the eclipse time and state of battery of the first period, and at the third period, we can predict whether the charge state is full or not.

In the battery discharge mode of the eclipse period, the change of battery capacity is same as Eq. (4). According to the result of DOD(Depth of Discharge) analysis during eclipse, the battery DOD is 72.5% without arcjet burn and is 75% with the arcjet burn as

Table 3 Predicted operating temperature of battery

Case / Temp	Operation Limits(℃)		Predicted Operating Temp(℃)		Operating Temp Margin(℃)	
	Min	Max	Min	Max	Min	Max
Beginning of Life, Autumnal Equinox	-10	45	-8	25	2	20
End of Life, Summer Solstice	-10	45	-8	13	3	32
End of Life, Winter Solstice	-10	45	-8	17	2	28

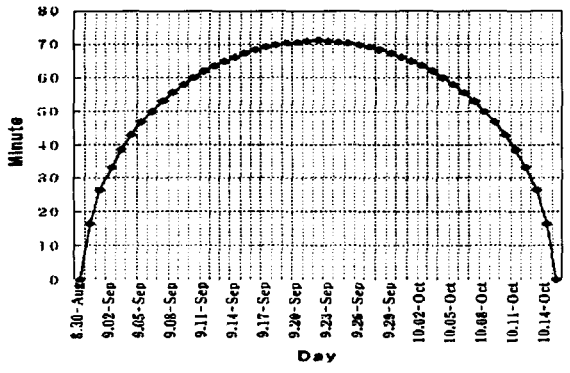

Fig. 10 Annual eclipse duration length

shown in Figs. 12(a), (b). This analysis results show good correction comparing to the data in Figs. 11(a), (b) as they are results of LMC(Lockheed Martin Company) analysis. Figures 12(a), (b) show the battery voltage profiles of the normal mode during arcjet implementation mode at the eclipse. At the second period of Fig 12(b), 2162 minutes, we can see that the battery SOC is instantly dropped with 12 minutes arcjet burn.

3.3 Worst case analysis mode

Eclipse failure mode is an analysis mode considering solar array circuit and battery cell failure. The solar array of Koreasat 3 is composed of 8 panels; 7 panels with silicon cell and 1 panel with GaAs cell. A silicon solar panels have totally 12 strings for a panel and 4 strings constitute a circuit. On the contrary, the GaAs panel has 21 strings and each 7 strings form a circuit. When a string or circuit failure occurs more large time for battery charge is needed. Table 4 presents a solar array power and margin rate, a battery DOD analysis data for the normal and failure modes, respectively. This mode presents the worst case caused by the solar array circuit failure or battery cell failure during the eclipse. The demanded battery power and the analysis results by this data are presented in Table 5. If the demanded power by the load is the same, the battery charge power decreases during charge after eclipse. When the arcjet is implemented during the charge, the overall power produced by the solar array and battery will decrease. In the eclipse failure mode, the analysis results are shown in Figs. 14(a), (b). This results are compared to Fig. 13(a), (b) where the battery state is analyzed using real test data. From the analysis result

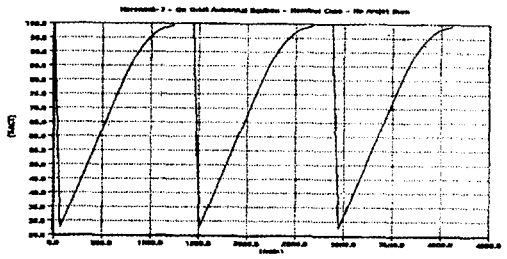

(a) Normal mode(no arcjet)

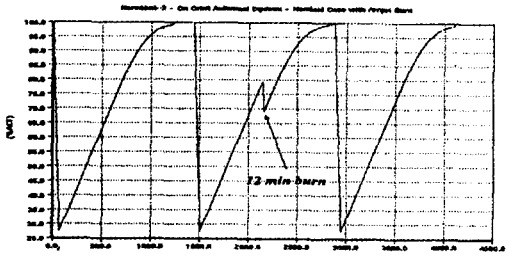

(b) Normal mode with arcjet burn

Fig. 11 Battery operation mode analysis at Autumnal Equinox (Lockheed Martin Analysis Results)

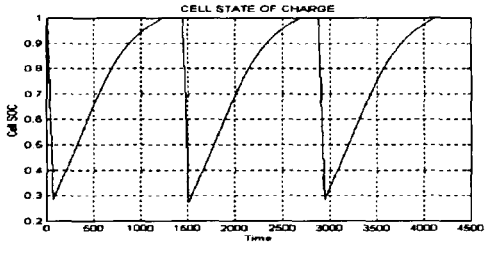

(a) Normal mode(no arcjet)

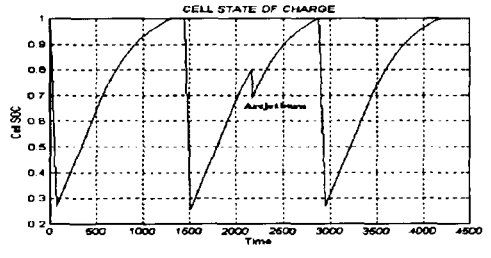

(b) Normal mode with arcjet burn

Fig. 12 Battery SOC status (Autumnal Equinox)

Table 4 Solar array power analysis data at Autumnal Equinox

Item \ Mode	Normal Mode	Normal Arcjet Mode	GaAs Circuit Fail Mode	Silicon String Fail Mode	Battery Cell Fail Mode
Solar Array Power	5120W	5120W	4826W	4967W	5120W
Solar Array Power Margin	375.3W	368.6W	0W	254.8W	350.3W
Solar Array Power Margin rate	7.33%	7.2%	0%	5.13%	6.6%
Battery DOD Results	72.6%	72.6%	72.5%	72.6%	76%

Table 5 Battery power analysis data at Autumnal Equinox

Item \ Mode	Normal Mode	Normal Arcjet Mode	GaAs Circuit Fail Mode	Silicon String Fail Mode	Battery Cell Fail Mode
Demanded Battery Power	3617W	3623.6W	3911W	3770W	350.3W
Battery Charge Rate	C/18	C/17.8	C/16	C/16	C/16
Battery DOD Analysis Results	72.5%	72.5%	72.5%	72.5%	75%

of Figs. 14(a), (b), when the solar array power decreases about 50W for the failure of solar array string with GaAs at the autumnal equinox, the battery DOD is 72.5%. For the failure of solar array circuit with silicon, the power is decreased about 353.4W with the battery DOD of 72.5%. Likewise, DOD is the same at the solar array string and circuit failure modes. From this results, we can see that the battery DOD at the autumnal equinox is not different between solar array string failure with GaAs and solar array circuit failure with silicon. But, in the failure mode, when the battery recharge, the charge rate is changed from C/18 to C/16 and the arcjet burn time is also changed from 12 minutes to 20 minutes by the solar array power decrease. Thus the battery power state is almost remains unchanged at the failure mode of the solar array string and circuit but the solar array margin approaches near zero during the battery charging .

In case of the battery cell failure mode, the battery impedance is reduced by decreasing the battery cell number. Also, the battery discharge current is increased so that the battery power to be provided to the load is increased and the battery power will be at lower DOD

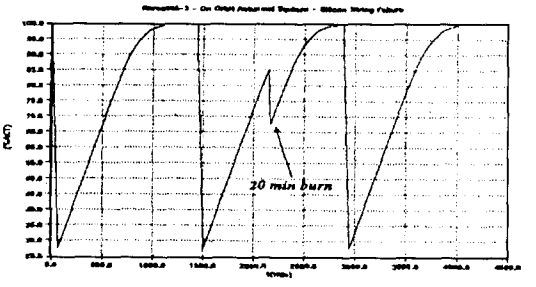

(a) Solar array string failure mode

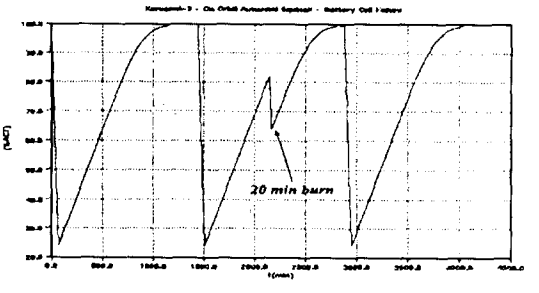

(b) Battery cell failure mode

Fig. 13 Battery operation mode analysis at Autumnal Equinox (Lockheed Martin analysis results)

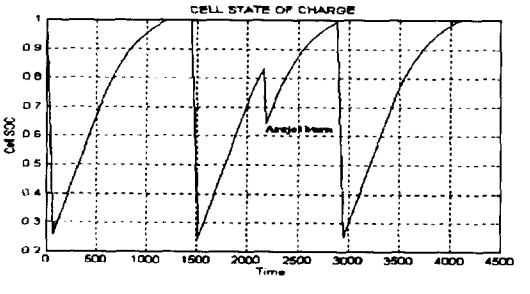

(a) Solar array string failure mode

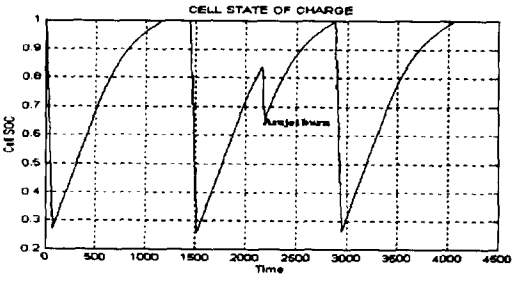

(b) Battery cell failure mode

Fig. 14 Battery operation mode analysis at Autumnal Equinox

state. The analysis result has 75% DOD in the failure mode of battery cell.

4. CONCLUSIONS

In this paper, the NiH_2 battery modeling using MNN is implemented, and the modeled numerical data are used for the analysis of the battery state during the eclipse. The results of neural network learning using the experimented data are shown at each different temperature point. The analysis results of the battery charge states according to operational modes, which are classified into the normal and failure modes, are presented and also the results are verified through comparison with the results where battery test data are provided by LMC.

The normal mode is analyzed during the eclipse with the arcjet burn and failure mode is also analyzed for the solar array string, solar array circuit and battery cell failure. The understanding of characteristics and SOC analysis of the NiH_2 battery will be helpful for the stable and successful operation of the satellite during satellite life time.

REFERENCES

[1] G. B. Jeong et al., "Battery modeling and power analysis of Koreasat", Journal of The Korean Society for Aeronautical and Space Sciences, Vol. 23, No. 6, pp.159~167, 1995.

[2] J. B. Kim, T. V. Nguyen, and R. E. White, "Thermal characteristics of a Nickel-Hydrogen battery", J. Electrochem, Soc., Vol. 141, No. 2, Feb., pp.333~338, 1994.

[3] A. H Zimmerman and M. V. Quinzio, "Progress towards computer simulation of NiH2 battery performance over life", The NASA Aerospace Battery Workshop, pp.177~183, 1994.

[4] A. H Zimmerman and M. V. Quinzio, "Nickel Hydrogen and Silver Zinc battery cell modeling at the Aerospace Corporation", The NASA Aerospace Battery Workshop, pp.439~446, 1995.

[5] Pauline De Vidts, Javier Delgado and Ralph E. White, "Mathematical modeling of a Nickel-Hydrogen cell", The NASA Aerospace Battery Workshop, pp.447~487, 1995.

[6] J. D. Dunlop, G. M. Rao and Thomas Y. Yi, NASA handbook for Nickel-Hydrogen batteries, NASA Reference Publication, 1993.

[7] J. D Choi et al., "Design and analysis of a battery charge/discharge regulator of satellite", The International Conference on Electrical Engineering, Vol. 2, pp.935~938, 1998.

〈저 자 소 개〉

최재동(崔載東)

1967년 11월 25일생, 1993년 충남대학교 전기공학과 졸업(학사), 1995년 동 대학원 졸업(석사), 1998년 동 대학원 박사과정수료, 1995년~1996년 한국과학기술원 인공위성 연구센터 연구원, 현재 한국항공우주연구소 선임연구원.

황영성(黃永聖)

1949년11월25일생, 1972년 홍익대학교 전기공학과 졸업(학사), 1991년 연세대학교 대학원 전기공학과 졸업(석사), 1998년 충남대학교 대학원 박사과정수료, 현재 국방과학연구소 책임연구원/팀장.

이학주(李鶴周)

1966년12월5일생, 1989년 충남대학교 전기공학과 졸업(학사), 1991년 동 대학원 전기공학과 졸업(석사), 1997년 동 대학원 박사과정수료, 현재 한전 전력연구원 전력계통연구실 연구원.

성세진(成世鎭)

1948년 7월 15일생, 1973년 서울대 공대 공업교육과 졸업(학사). 1975년 동 대학원 졸업(석사). 1988년 일본 동경공업대 대학원 졸업(박사). 현재 충남대 공대 전기공학과 교수. 당 학회 감사.